Fluid Phase Equilibria 302 (2011) 310–315

Contents lists available at ScienceDirect

Fluid Phase Equilibria

journal homepage: www.elsevier.com/locate/fluid

Wetting transition of water on graphite and boron-nitride surfaces: A molecular dynamics study

Ravi C. Dutta, Sandip Khan, Jayant K. Singh*

Department of Chemical Engineering, Indian Institute of Technology Kanpur, Kanpur 208016, India

ARTICLE INFO

Article history:
Received 3 June 2010
Received in revised form 6 July 2010
Accepted 8 July 2010
Available online 15 July 2010

Keywords:
Contact angle
Wetting temperature
Line tension
Graphite
Boron-nitride

ABSTRACT

Wetting transition of water on graphite and boron-nitride (BN) surfaces is investigated by molecular dynamics simulation. In particular, we report the effect of temperature and system size on the contact angle of water droplet on the two surfaces. Wetting temperature of water on graphite is found to be 470 ± 5 K, which is in good agreement with the estimate of Zhao (Phys. Rev. B 76 (2007) 041402) using grand-canonical Monte Carlo simulations. On the other hand, wetting temperature of water on BN surface is estimated to be lower, 438 ± 5 K. Temperature dependence of line tension of water droplet on both the surfaces is also studied, and found to vary between 10^{-10} and 10^{-9} N for temperature in the range of 300–420 K. In this work, line tension for water on graphite and BN surfaces is observed to have a logarithmic proportional behavior with the contact angle.

1. Introduction

Wetting behavior of fluid–solid interfaces is of practical interest to technological important areas such as sensors [1] and coatings [2]. Wetting of patterned surfaces by liquids plays a key role in the fields of nanofluidics [3,4] and biophysics [5]. Increase in demand of nano-based technologies requires having a clear picture of wetting behavior on functional surfaces. Despite the potential of controlling the wettability to transform the nano-based device radically, we are yet to devise a practical way to make smart surfaces.

Wettability of solid surface is a characteristic property of materials. It strongly depends on both surface energy and surface roughness and is characterized invariably by the contact angle, θ, which is given by the following Young's relation [6]:

$$\gamma_{LV} \cos\theta = \gamma_{SV} - \gamma_{SL}, \quad (1)$$

where γ_{SL}, γ_{LV} and γ_{SV} are interfacial free energies per unit area of the solid–liquid, liquid–vapor and solid–vapor, respectively.

Wetting transition is characterized usually by the wetting temperature at which drop vanishes and wets the surfaces completely. Various works have been done in order to understand the wetting transition by experiments [7,8]. Previous theoretical studies reveal that variety of simple and associating fluids undergoes the first-order wetting transition [9–11]. Surprisingly, the experimental evidence is very limited [12–14], due to sensitivity of contact angle to impurities/defects on the surface. Experimental observation of the contact angle of water on a graphite surface [15] at the room temperature ranges from 60° to 80°, which illustrates experimental difficulties to study such phenomena. In addition, impurities and defects of surface are unavoidable in experiment [16], which essentially changes the interfacial water behavior.

On the other hand, molecular simulation, based on molecular interaction model, can explore the behavior of fluid near the surface systematically. Various workers have done some work in this direction. For example, Pertsin and Grunze [17] studied the behavior of water confined between two graphite sheets, while Muller et al. [18] performed a Monte Carlo study on adsorption of water on activated carbons. Zhao [19] recently studied the prewetting transition of water on a graphite surface. A number of MD studies are also performed to understand the droplet dynamics on solid surfaces. For instance, Hautman and Klein [20] investigated the microscopic wetting of hydrophilic and hydrophobic surfaces with terminal function groups. Lundgren et al. [21] studied the wetting behavior of water and water/ethanol mixture on graphite surface, without considering system size effects and obtained a microscopic contact angle of 83° for water on graphite surface; while Werder et al. [22] studied contact angle of water on a graphite surface by varying interaction parameters. On the other hand, Zangi and Berne [23] investigated the dependency of temperature on contact angle of water droplet on a graphite surface. Subsequently, number of molecular dynamics studies are performed on the contact angle of water droplet on different surfaces such as TiO_2 surface [24] and amorphous silica surface [25]. Similar wetting studies have been done for silver on nickel surface [26] and aqueous trisilox-

* Corresponding author.
E-mail address: jayantks@iitk.ac.in (J.K. Singh).

0378-3812/$ – see front matter © 2010 Elsevier B.V. All rights reserved.
doi:10.1016/j.fluid.2010.07.006

Table 1
Lennard–Jones parameters.

Pair	σ (Å)	ε (kJ/mol)	q (e)
OW–OW [41]	3.1666	0.6502	−0.8476
HW–HW [41]	0	0	+0.4238
C–OW [22]	3.190	0.392	0
B–B [61]	3.453	0.3971	0
N–N [61]	3.365	0.6060	0

ane and alkyl polyethoxylate surfactant solutions on a graphite substrate [27]. In all the above studies, investigation related to wetting temperature and line tension is missing. This is, in fact, the main objective of the current study. In this work, we present a systematic study of wetting transition and line tension of water droplet on graphite and boron-nitride surfaces. Such materials in different shapes such as nanotubes and fullerenes, have shown substantial evidence of extraordinary hydrodynamic behavior of water [28–37]. We expect that the current work will find use in future studies pertinent to the field of biosensors and nanofluidics.

The rest of the paper is organized as follows: in the next section, we describe the model and methods employed in this work. Section 3 presents the results on the effect of system size and temperature on the contact angle of water on graphite and BN surfaces. In addition, we report the line tension, which for the first time, to our best knowledge, is investigated systematically using molecular dynamics. Section 4 summarizes the work.

2. Computational model and method

2.1. Model

Molecular dynamic simulations are carried out under constant number of particles N, volume V, and the temperature T (NVT ensemble). In this work, we have used DLPOLY [38]. Graphite and BN surfaces are constructed by periodically replicating the unit cell in lateral directions. The graphite surface consists of two layers of carbon atoms separated by 1.53 Å and the distance between the layers is 3.4 Å. Cutoff radius of 10 Å is used to omit the effect of additional number of surface layers. The BN surface consists of alternating boron and nitrogen atoms in a graphite like sheet with almost no change in atomic spacing [39]. The surface atoms are kept frozen during simulations. The dimensions of the box varied from 150×150 to 200×200 Å^2 depending on the size of the droplet. The substrate size is sufficiently large to remove the effect of periodic images of the droplet in lateral directions. The height of the simulation box is taken as 270 Å to avoid any interaction of periodic image of the droplet [40].

Water–water interaction is described by the SPC/E [41] model in which the hydrogen's are located at 1 Å from the oxygen with an H–O–H angle of 109.47°. Bond distance and bond angle are fixed throughout the simulation with the SHAKE algorithm [42]. The intermolecular interaction in the SPC/E model is defined as:

$$U_{LJ}(r_{ij}) = 4\varepsilon \left[\left(\frac{\sigma}{r_{ij}} \right)^{12} - \left(\frac{\sigma}{r_{ij}} \right)^{6} \right] + \sum_{i=1}^{3} \sum_{j=1}^{3} \frac{q_i q_j}{r_{ij}}, \tag{2}$$

where r_{ij} is the distance between any pair of atoms i and j, σ represents the atom size, ε is the interaction energy depth between two atoms and q_i and q_j are the charges centered on the individual atoms of different water molecules. Surface–water interaction is represented by Lennard–Jones potential and the corresponding interaction parameters are calculated using the Lorentz–Berthelot mixing rules as shown in Table 1: $\sigma_{ij} = (\sigma_i + \sigma_j)/2$ and $\varepsilon_{ij} = \sqrt{\varepsilon_i \varepsilon_j}$.

Initial configuration is generated by placing water molecules, in the range 2000–7000 particles, on a cubic lattice. Subsequently, water cubic structure is kept on the surface at the bottom of the simulation box. The lateral dimension of box is the same as that of the surface. Each simulation is carried out for 1.2 ns with an integration time of 2 fs with 0.6 ns as equilibration run length and equal amount for the production run. The Nose–Hoover thermostat is used to maintain the system temperature with relaxation constant of 1.0 ps. Electrostatic interactions are incorporated using the single particle mesh Ewald method [43].

2.2. Methodology

Graphical binning approach is considered to calculate various properties such as vapor–liquid densities and contact angles. In this approach, we assume azimuthal symmetry in the droplet and introduce the cylindrical coordinate system (r, z), where r is the distance from the z-axis. Such approach was earlier used by Werder et al. [22] and Aluru and co-worker [24]. We have considered the top most surface layer for the zero reference level and the surface normal through the center of mass of the droplet as the reference axis. The bins have a height of 1 Å and are of equal volume, i.e., the radial bin boundaries are located at $r_i = \sqrt{(i\delta A/\pi)}$ for $i = 1, \ldots, N$ bins with a base area per bin of $\delta A = 95$ Å^2. Contact angle is extracted from a two-step procedure from the profiles as described by de Ruijter et al. [44]. First, the location of the equimolar dividing surface is determined within every single horizontal layer of the binned drop. Second, a circular best fit through these points is extrapolated to the surface where the contact angle θ is measured. The boundary between equilibrated liquid and vapor interface for a given droplet is determined at the position where the density is half of bulk water density and is modeled using the relation for liquid–gas interface:

$$\rho(r) = \frac{1}{2}\left(\rho^L + \rho^V\right) - \frac{1}{2}\left(\rho^L - \rho^V\right) \tan h\left(\frac{2(r - r_e)}{d}\right), \tag{3}$$

where ρ^L and ρ^V are liquid and vapor densities, respectively, r is the distance from origin to the droplet surface, r_e is the center of the interface region, and d is the interface thickness. The points of the equimolar surface below a height of 8 Å from the graphite or BN surface are not taken into account for the fit, to avoid the influence of density fluctuations at the liquid–solid interface.

The size of the droplet influences the wetting behavior when used as nanoscale droplets such as in microelectronic systems and microfluidic devices [45]. To determine the effect of droplet size on the microscopic contact angle we have utilized the following modified Young's equation:

$$\gamma_{SV} = \gamma_{SL} + \gamma_{LV} \cos\theta + \left(\frac{\tau}{r_B}\right), \tag{4}$$

where τ and r_B are line tension and radius of the droplet, respectively.

Macroscopic contact angle can be derived for infinitely large drop, i.e., $1/rB \to 0$, which yields a well known Young's equation (Eq. (1)):

$$\cos\theta_\infty = \left(\frac{\gamma_{SV} - \gamma_{SL}}{\gamma_{LV}}\right).$$

Eq. (4) can be rewritten in terms of macroscopic contact angle and line tension as shown below:

$$\cos\,\theta = \cos\theta_\infty - \left(\frac{\tau}{\gamma_{LV}}\right)\frac{1}{r_B}. \tag{5}$$

A series of finite size contact angles can be used along with Eq. (5) to obtain the macroscopic contact angle.

Hydrogen bond (HB) plays a crucial role in the behavior of water as their spatial patterns and fluctuations characterize the structure and dynamics of the liquid [46]. In this work, we perform HB analysis, using the geometrical criteria as described by Swiatla-Wojcik

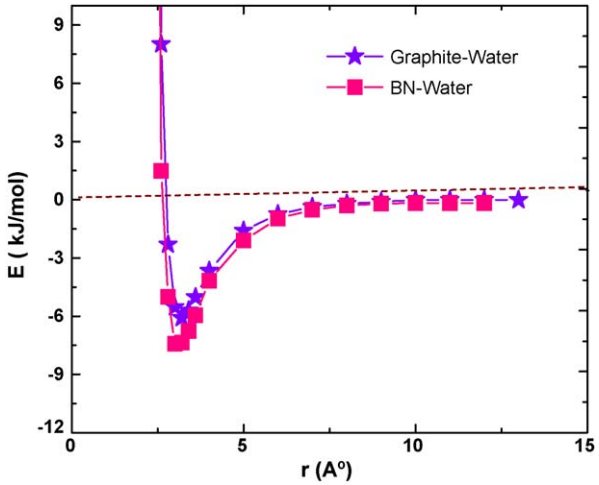

Fig. 1. Effective potential of water–graphite and water–BN systems. Symbols star and square represent water–graphite system and water–BN system, respectively.

[47] to understand the effect of temperature and surface on the HB static distribution.

3. Results and discussion

Fig. 1 displays the effective water-surface potential energy for the graphite and BN surfaces. To evaluate the effective interaction, we place a water molecule with different orientations at different distances from the surface. For graphite–water system $\sigma_{\text{graphite–water}} = 3.2$ Å and $\varepsilon_{\text{graphite–water}}$ of -6.1 kJ/mol obtained in this work is in good agreement with previous reported values, 3.19 Å and -6.31 kJ/mol [48,49], respectively. For BN–water system we obtained $\sigma_{\text{BN–water}}$ and $\varepsilon_{\text{BN–water}} = 3.0$ Å, -7.43 kJ/mol, respectively. These effective interaction parameters between BN sheet and water are dependent on the mixing rule. In this work, we have considered Lorenz–Berthelot rule for obtaining the values of interaction parameters for B–OW and N–OW. Hence, all the results of BN–water system obtained in this work are based on the above approximation.

We start our discussion with Fig. 2, which presents water density profiles at different temperatures for graphite–water system (Fig. 2(a)) and density profiles for BN–water system (Fig. 2(b)). The liquid density (ρ_L) and vapor density (ρ_V) are calculated from Eq. (3) as per methodology described in the previous section. Fig. 2 clearly indicates that the surface effect exists up to some molecular distance due to which the density has an oscillatory nature. For the graphite–water system, two pronounced density peaks are observed at 300 K, close to the surface, with peak heights of 1.61 and 1.13 g/cm^3 at a distance of 2 and 5 Å, respectively from the surface. On the other hand, for BN–water system, the corresponding two density peaks are observed at a distance of 3 and 6 Å from the surface, with densities = 1.546 and 1.09 g/cm^3, respectively, at 300 K. Subsequent to the fluid adsorbed layers, the liquid density approaches that of the bulk value before reaching the vapor–liquid interfacial region. We have performed such calculations for various temperatures. Saturated liquid densities obtained from the density profile at 300, 325, 350, 375, 400 and 420 K are 0.996 ± 0.02, 0.978 ± 0.02, 0.944 ± 0.02, 0.9224 ± 0.02, 0.9084 ± 0.02 and 0.8654 ± 0.02 g/cm^3, respectively. These values are in excellent agreement with that of bulk water densities, for SPC/E model, as reported by Vega and Miguel [50].

In order to understand the hydrogen bond dynamics near the surface, we examined the variation of hydrogen bonds with temperature. As per the methodology described by Swiatla-Wojcik

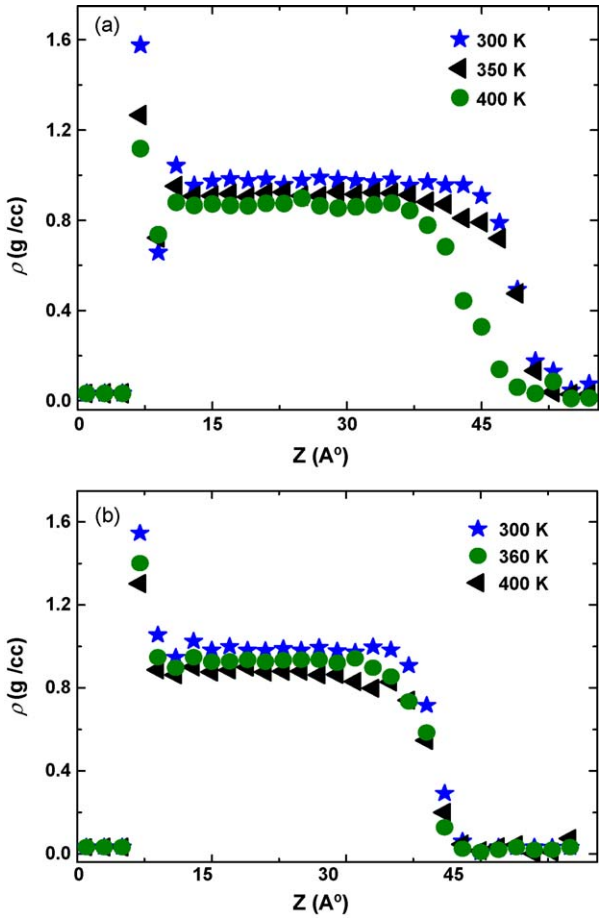

Fig. 2. (a) Density profiles of water on graphite surface along the centerline of the droplet at different temperatures. Symbols square, circle, and triangle represent 300, 375, and 420 K, respectively. (b) Density profiles of water on BN surface along the centerline of the droplet at different temperatures. Symbols circle, star, and triangle represent 300, 360, and 400 K, respectively.

[47], the HB analysis requires cutoff values for O–O and O–H distances between different molecules. We have obtained these values from the radial distribution function calculation (figure not shown for brevity). At 300 K the average number of HB per water molecule, in the bulk region, is 3.40 ± 0.05, which is in agreement with the previously reported [24] value of 3.5 hydrogen bonds per water molecule on titanium dioxide surface at the same temperature. To analyze the effect of system size on the HB analysis, we carried out various simulations, with different system sizes, to understand the change in hydrogen bond at different temperatures. Fig. 3(a) describes a graph between $1/N_{\text{wt}}$ and P ($n_{\text{HB}} = 1$) for different temperatures. Here N_{wt} is number of water molecules in the system and P ($n_{\text{HB}} = 1$) is defined as the probability to find an atom with one hydrogen bond. System size is found to have very less effect on HB. Similar behavior is observed for higher order P ($n_{\text{HB}} > 1$) of hydrogen bond. We used such analysis to obtain the HB distribution for infinitely large drop, P_{inf} (n_{HB}). Fig. 3(b) shows the behavior of P_{inf} (n_{HB}) at different temperatures for a water drop on the graphitic surface. As we increase the temperature P_{inf} ($n_{\text{HB}} = 1$–3) increases; on the other hand P_{inf} ($n_{\text{HB}} = 4, 5$) decreases with increasing temperature. Similar behavior is observed for the HB distribution as a function of temperature for water on the BN surface.

One of the main objectives in this work is to obtain the contact angle behavior of water on the two surfaces, graphite and boron-nitride, for different temperatures. Contact angle is primarily sensitive to the characteristic energy of fluid–wall interaction as

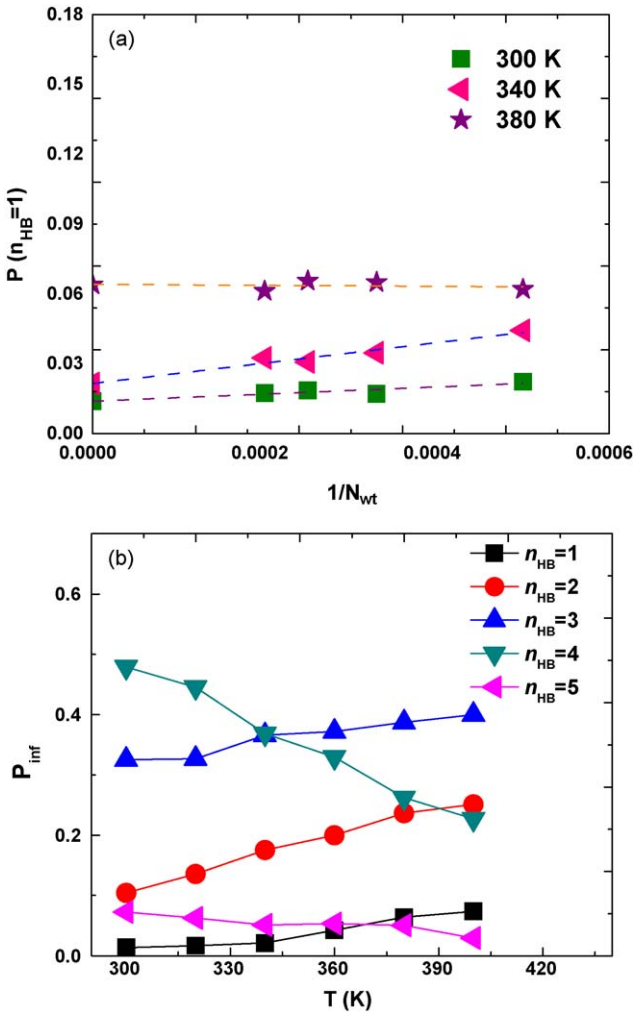

Fig. 3. (a) System size effect on hydrogen bond at various temperatures. Symbols square, triangle and star represent 300, 340, and 400 K, respectively. (b) Probability (P_{inf}) to find a water molecule with hydrogen bonds at different temperatures. Symbols square, circle, triangle up, triangle down, triangle left represent probability to find an atom having 1, 2, 3, 4 and 5 hydrogen bonds, respectively.

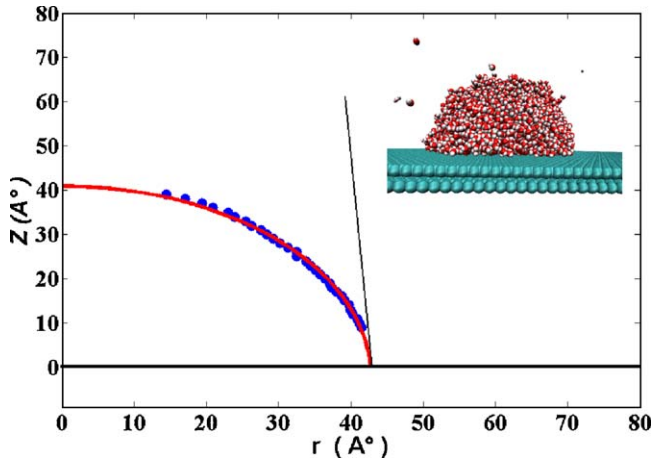

Fig. 4. Schematic for the computation of contact angle for graphite–water system at 300 K.

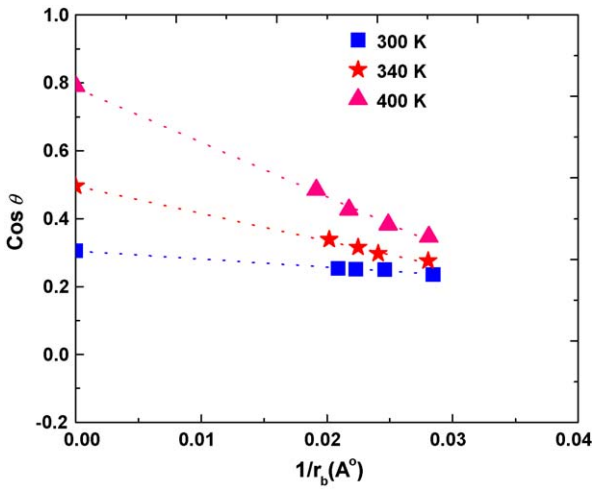

Fig. 5. Dependence of the system size on contact angle of water droplet on the BN surface at different temperatures. Symbols square, star, and triangle represent contact angles at 300, 340, and 400 K, respectively. Data points, from right to left, represent droplet with 2000, 3000, 4000, 5000 water molecules.

shown by Werder et al. [22] in detail. We have chosen the parameters from the work of Werder et al. [22], which have yielded the contact angle value close to that seen in recent experiments. Eq. (5) clearly indicates that the microscopic contact angle depends on the drop size. Such dependencies have been observed in various experiments [51–53]. Hence, it is imperative to consider the effect of system size on the contact angle. For each temperature, we have simulated four to five system sizes ranging from 2000 to 7000 water molecules. In order to retain the structure of the drop, substrate area is also accordingly modified. Note that the layered structure of the liquid close to the wall ($0 < z < 8$ Å) is neglected in the contact angle measurement. Fig. 4 represents the pictorial form of water droplet on the graphitic surface and the fitting representation of the drop, which is used to obtained the contact angle of the droplet.

Fitting method, as described in the previous section, is applied to calculate the contact angle for various system sizes. System size effects are found to be significant at relatively higher temperature. For example, the variation in contact angle at 300 K for a system size of $N_{wt} = 4000$ to $N_{wt} = 7000$ is around 3°; on the other hand, the corresponding variation is around 8° at 400 K. Fig. 5 presents the cosine of the microscopic contact angle vs. inverse of the drop radius, i.e., $\cos\theta$ vs. $1/r_B$. Fig. 5 clearly illustrates the linear relation of the contact angle to the inverse of the drop radius as suggested by Eq. (5).

A straight line is fitted to the data and extrapolated to the infinite radius for obtaining the true or macroscopic contact angle, θ_∞. Similar extrapolation technique from series of finite system size simulations is employed to obtain contact angles at various temperatures for water on BN and graphite surfaces. Table 2 summarizes the contact angle for various temperatures for both surfaces. Wetting temperature, T_W, is evaluated from a series of contact angles

Table 2
Variation of contact angle and line tension with temperature for graphite–water and BN–water systems.

T (K)	θ_{GW} (°)	θ_{BN} (°)	$\tau_{G\text{–water}}$ (10^{-10} N)	$\tau_{BN\text{–water}}$ (10^{-10} N)
300	83(2)	73(1)	3.0(3)	2.3(2)
320		67(2)		3.0(2)
325	76(2)		5.0(3)	
340		61(2)		4.1(2)
350	69(2)		6.5(4)	
360		55(3)		4.8(3)
375	61(2)		8.1(4)	
380		45(3)		6.8(3)
400	52(3)	37(3)	10.5(5)	9.0(3)
420	41(4)		12.5(5)	

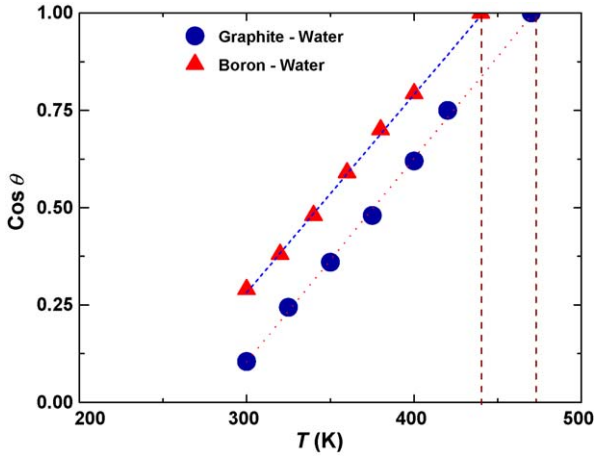

Fig. 6. Dependency of cosine of macroscopic contact angle θ against temperature for graphite–water and BN–water systems. Dashed line along the data points is guide to the eye. Dashed vertical lines represent the estimated wetting temperatures. Error bars are smaller than the symbol size.

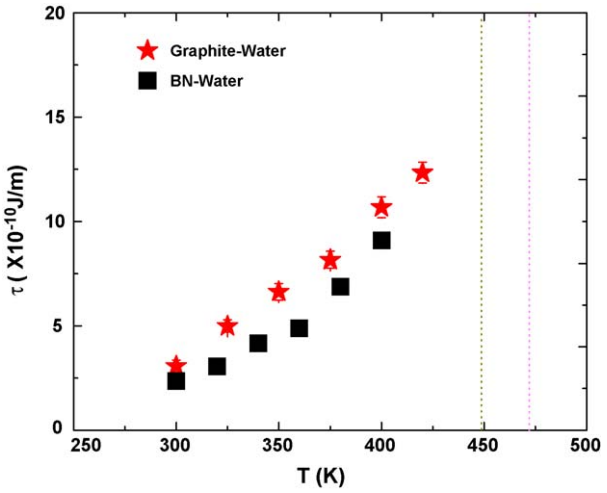

Fig. 7. Line tension vs. temperature for graphite–water and BN–water systems.

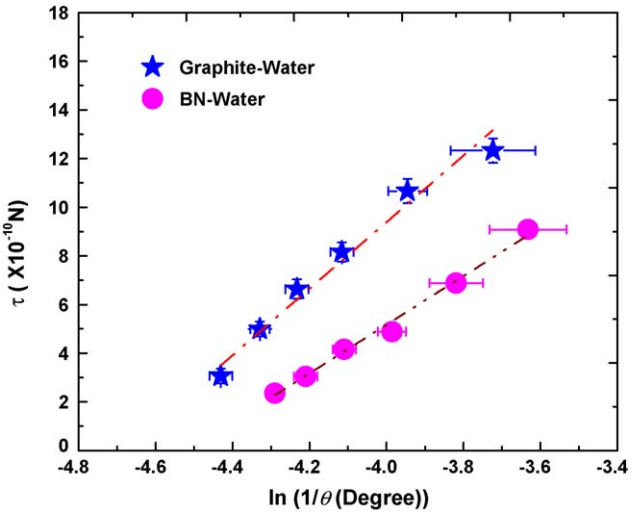

Fig. 8. Line tension vs. $\ln(1/\theta)$ for graphite–water and BN–water systems where θ is in degree. Dashed and dotted lines are guide to the eye.

as a function of temperature. The data is extrapolated linearly to obtain the temperature at which contact angle becomes zero as described in Fig. 6.

In this work, T_W for the graphite–water system is 470 ± 5 K. On the other hand, T_W for the BN–water system is found to be relatively lower, 438 ± 5 K. Our estimate of wetting temperature of water on the graphite surface is in agreement with that obtained from the GCMC simulation of Zhao [19]. It may be pointed out that these are the theoretical estimates and the experimental measurements in this respect are not available.

In this work, we have also investigated the behavior of line tensions from MD. Line tension affects the stability of emulsion and foams and would play an important role in micro/nanofluidic devices. As summarized by Amirfazli and Neumann [54], line tension has been found to be negative as well as positive. In order to calculate the line tension for current systems, at a certain temperature, we obtain the slope, $-\tau/\gamma_{LV}$, from the system size analysis data as shown in Fig. 5. The numerical values for γ_{LV} are taken from the study by Vega and Miguel [50] for SPC/E water at different temperatures. The calculated values are in the order of 10^{-10} N in this work and are in good agreement with the order of the line tension value reported in the literature [55,56]. We obtained 3.06×10^{-10} N as the line tension value at 300 K, which is in good agreement with the previously reported values for graphite–water system at the same temperature by Werder et al. [22]. In a recent work, Zangi and Berne [23] assumed a constant line tension for different temperatures for their study of water on a hydrophobic plate. On the contrary, in this work, the line tension is found to substantially increase with increasing temperature. The variation of the line tension for water on graphite and BN surfaces is shown in Fig. 7.

In general, there is a consensus of positive line tension near first-order wetting [57]. At wetting, short-ranged interactions are characterized by a finite τ with finite slope, while the retarded van der Waals interactions exhibit finite τ with diverging slope, and the longer ranged interactions (e.g., non-retarded van der Waals) exhibit diverging τ. However, which of the two forces (long or short ranged) dominate cannot be ascertained from the calculated line tension data. Fig. 8 describes the graph of τ vs. $\ln(1/\theta)$, which yields a straight line. The behavior of line tension against contact angle is in agreement with that from the theories proposed by Joanny and Gennes [58,59] as well as by Churaev et al. [60]. In particular, these theories suggest that τ is positive near wetting temperature and diverges as T approaches the T_W, following a logarithmic relation with the contact angle, i.e., $\tau(\theta) \alpha \ln(1/\theta)$. Interestingly, slope of the linear fit as in Fig. 8 for water on BN and graphite surfaces are slightly different with relatively larger value observed for the graphitic surface owing to its relatively hydrophobic nature. However, the line tension behavior of water on BN and graphite surfaces is similar at lower temperature (see Fig. 7). Nevertheless, the behavior substantially changes at higher temperature where the line tension of water on BN surface appears to diverge earlier than that for the graphite surface.

4. Conclusions

We investigated the wetting behavior of water droplet on graphite and boron-nitride surfaces using MD simulations. We systematically studied the effect of temperature and system size on the contact angle of water droplet on both surfaces. We reported, for the first time to the best of our knowledge, the temperature dependency of line tension. The wetting temperature of water on graphite is found to be 470 ± 5 K, which is in agreement with the predicted value from the grand-canonical Monte Carlo simulations. On the other hand, the wetting temperature of water on boron-nitride is estimated to be relatively lower, 438 ± 5 K. HB distribution is studied to understand its variation at different temperatures. The behavior of HB distribution of water near both surfaces is found to

be characteristically similar. The line tension for the systems studied is observed to be logarithmically proportional to the contact angle.

Acknowledgements

This work was supported by the Department of Science and Technology, Govt. of India (Grant No. SR/S3/CE/061/2009), Council of Scientific and Industrial Research (Grant No. and) UP-Council of Science and Technology (Grant No. CST/SERPD/D-3206).

References

[1] B.F. Erlanger, B.X. Chen, M. Zhu, L. Brus, Nano Lett. 1 (2001) 465–467.
[2] A. Reisch, J.C. Voegel, E. Gonthier, G. Decher, B. Senger, P. Schaaf, P.J. Msini, Langmuir 25 (2009) 3610–3617.
[3] J.C. Rasaiah, S. Garde, G. Hummer, Annu. Rev. Phys. Chem. 59 (2008) 713–740.
[4] C.Y. Won, N.R. Aluru, J. Phys. Chem. C 112 (2008) 1812–1818.
[5] E. Sackmann, R.F. Bruinsma, Chemphyschem 3 (2002) 262–269.
[6] Y.T. Phiylos, Trans. R. Soc. Lond. 95 (1805) 65.
[7] S. Kwon, R. Vidic, E. Borguet, Surf. Sci. 522 (2003) 17–26.
[8] G. Nagy, J. Electroanal. Chem. 409 (1996) 19–23.
[9] C. Ebner, W.F. Saam, Phys. Rev. Lett. 38 (1977) 1486.
[10] J.W. Cahn, J. Chem. Phys. 66 (1977) 3667.
[11] A. Patrykiejew, S. Sokołowski, J. Phys. Chem. B 103 (1999) 4466–4473.
[12] R.B. Hallock, J. Low Temp. Phys. 101 (1995).
[13] J.E. Rutledge, P. Taborek, Phys. Rev. Lett. 69 (1992) 937.
[14] J.A. Phillips, D. Ross, P. Taborek, J.E. Rutledge, Phys. Rev. B 58 (1998) 3361.
[15] M.E. Tadros, P. Hu, A.W. Adamson, J. Colloid Interface Sci. 49 (1974) 184–195.
[16] I.N. Kholmanov, L. Gavioli, M. Fanetti, M. Casella, C. Cepek, C. Mattevi, M. Sancrotti, Surf. Sci. 601 (2007) 188–192.
[17] A. Pertsin, M. Grunze, J. Phys. Chem. B 108 (2004) 1357–1364.
[18] E.A. Muller, L.F. Rull, L.F. Vega, K.E. Gubbins, J. Phys. Chem. 100 (1996) 1189–1196.
[19] X. Zhao, Phys. Rev. B 76 (2007).
[20] J. Hautman, M.L. Klein, Phys. Rev. Lett. 67 (1991) 1763–1766.
[21] M. Lundgren, N.L. Allan, T. Cosgrove, Langmuir 18 (2002) 10462–10466.
[22] T. Werder, J.H. Walther, R.L. Jaffe, T. Halicioglu, P. Koumoutsakos, J. Phys. Chem. B 107 (2003) 1345–1352.
[23] R. Zangi, B.R. Berne, J. Phys. Chem. B 112 (2008) 8634–8644.
[24] J.H. Park, N.R. Aluru, Mol. Sim. 35 (2009) 31–37.
[25] J. Chai, S. Liu, X. Yang, Appl. Surf. Sci. 25 (2009) 9078–9084.
[26] Y. Sun, E.B. Webb III, J. Phys.: Condens. Matter 21 (2009) 464135.
[27] J.D. Halverson, C. Maldarelli, A. Couzis, J. Koplik, Chem. Eng. Sci. 64 (2009) 4657–4667.
[28] M.C. Gordillo, J. Marti, Chem. Phys. Lett. 329 (2000) 341–345.
[29] A. Striolo, Nano Lett. 6 (2006) 633–639.
[30] A.I. Kolesnikov, C.K. Loonga, N.R. de Souza, C.J. Burnham, A.P. Moravsky, Physica B 385 (2006) 272–274.
[31] J.H. Walther, R. Jaffe, T. Halicioglu, P. Koumoutsakos, J. Phys. Chem. 105 (2001) 9980–9987.
[32] J.M.D. Leoa, J. Maranon, J. Mol. Struct. 709 (2004) 163–166.
[33] U. Zimmerli, P.G. Gonnet, J.H. Walther, P. Koumoutsakos, Nano Lett. 5 (2005) 1017–1022.
[34] J. Zang, S. Konduri, S. Nair, D.S. Sholl, ACS Nano 3 (2009) 1548–1556.
[35] D.R. Weiss, T.M. Raschke, M. Levitt, J. Phys. Chem. 112 (2008) 2981–2990.
[36] S. Supple, N. Quirke, Phys. Rev. Lett. 90 (2003) 214501.
[37] M.J. Longhurst, N. Quirke, Nano Lett. 7 (2007) 3324–3328.
[38] W. Smith, T.R. Forester, I.T. Todorov, The Dlpoly User Manual Version 2.19, SFTC Daresbury Laboratory, 2008.
[39] G. Ciofani, V. Raffa, A. Menciassi, A. Cuschieri, Nano Today 4 (2009) 8–10.
[40] E. Sophr, J. Chem. Phys. 107 (1997) 66342–66348.
[41] H.J.C. Berendsen, J.R. Grigera, T.P. Straatsma, J. Phys. Chem. 91 (1987) 6269–6271.
[42] S. Miyamoto, P.A. Kollman, J. Comp. Chem. 13 (1992) 952–962.
[43] T. Darden, D. York, L. Pedersen, J. Chem. Phys. 98 (1993) 10089–10092.
[44] M.J.d. Ruijter, T.D. Blake, J.D. Coninck, Langmuir 15 (1999) 7836–7847.
[45] D.R. Heine, G.S. Grest, E.B. Webb, Phys. Rev. Lett. 95 (2005) 107801–107804.
[46] A. Luzar, D. Chandler, Nature 379 (1996) 55–57.
[47] D. Swiatla-Wojcik, Chem. Phys. 342 (2007) 260–266.
[48] L.J. Richard, P. Gonnet, T. Werder, J.H. Walther, P. Koumoutsakos, Mol. Sim. 30 (2004) 205–216.
[49] R.J. Hernandez, J. Breton, J.M.G. Liorente, D.J. Wales, J. Phys. Chem. B 110 (2006) 13357.
[50] C. Vega, E.D. Miguel, J. Chem. Phys. 126 (2007).
[51] K.W. Stockelhuber, B. Radoev, H.J. Schulze, Colloids Surf. A: Physicochem. Eng. Aspects 156 (1999) 323–333.
[52] R.J. Good, M.N. Koo, J. Colloid Interface Sci. 71 (1979) 283–292.
[53] A. Amirfazli, D.Y. Kwok, J. Gaydos, A.W. Neumann, J. Colloid Interface Sci. 205 (1998) 1–11.
[54] A. Amirfazli, A.W. Neumann, Adv. Coll. Int. Sci. 110 (2004) 121–141.
[55] F. Mugele, T. Becker, R. Nikopoulos, M. Kohonen, S. Herminghaus, J. Adhes. Sci. Technol. 16 (2002) 951–964.
[56] J.S. Rowlinson, B.W. Widom, Molecular Theory of Capillarity, Clarendon Press, Oxford, 1982.
[57] J.O. Indekeu, J. Mod. Phys. B 8 (1994) 309–345.
[58] J.F. Joanny, P.G.d. Gennes, J. Colloid Interface Sci. 111 (1986) 94.
[59] J.F. Joanny, P.G.d. Gennes, C. R. Acad. Sci. (Paris) 303 (1986) 337.
[60] N.V. Churaev, V.M. Starov, B.V. Derjaguin, J. Colloid Interface Sci. 89 (1982) 16.
[61] J.W. Kang, H.J. Hwang, J. Phys.: Condens. Matter 16 (2004) 3901–3908.